28th SolarPACES Conference

Placeholder Session title

https://doi.or/10...... DOI placeholder (WILL BE FILLED IN BY TIB Open Publishing)

© Authors. This work is licensed under a Creative Commons Attribution 4.0 International License

Published: (WILL BE FILLED IN BY TIB Open Publishing)

Development of Self-Passivating, High Strength Ferritic Alloys for CSP and TES Application

Fadoua Aarab^{1[https://orcid.org/0000-0001-9495-7812]}, Bernd Kuhn^{2[https://orcid.org/0000-0002-7929-0711]}

¹ Institute of Energy and Climate Research (IEK), Structure and Function of Materials (IEK-2), Forschungszentrum Jülich GmbH, 52425 Jülich, Germany; b.kuhn@fz-juelich.de; Tel.: +49-2461-61-4132

Abstract. The addition of aluminium to ferritic stainless steels can result in self-passivation by the formation of a compact Al₂O₃ top layer, which exhibits significantly higher corrosion resistance to solar salt compared to a Cr₂O₃ surface layer. The development and qualification of realistic experimental methods for fatigue testing under superimposed salt corrosion attack will enable safe component design. Salt corrosion experiments were carried out at 600 °C with and without mechanical fatigue loading at a novel, self-passivating trial steel, using "solar salt" (60 wt.% NaNO₃ and 40 wt.% KNO₃) Furthermore, experiments within the framework of method qualification were carried out on the commercial materials TP347H and DMV 310N. Cyclic salt corrosion tests at 600 °C under flowing synthetic air (without mechanical loading) showed that self-passivation to molten salt attack and mechanical strengthening by precipitation of fine Laves phase particles is possible in novel ferritic HiperFer^{SCR} (Salt Corrosion Resistant) steel. A compact, continuous Al₂O₃ layer was formed on the surface of the model alloys with Al contents of 5 wt.% and higher. A distribution of fine, strengthening Laves phase precipitates was achieved in the metal matrix.

Keywords: Concentrating solar power, Salt corrosion resistance, Protective Al_2O_3 scale; Strengthening Laves Phase precipitation

Introduction

Solar tower power plants are one of the most promising renewable technologies for large-scale power and process heat generation [1]. Solar thermal power plants typically use molten salts for heat transfer and storage [2]. The so-called "solar salt" is a mixture of 60 wt.% NaNO $_3$ and 40 wt.% KNO $_3$ [3]. The overall efficiency of commercially operated solar thermal power plants is currently limited by the thermal stability of the solar salt, which makes process temperatures above 600 °C difficult [4]. Even at these temperatures, increased corrosion of metallic components occurs, requiring careful material selection [5]. Although the cost of solar thermal power plants has decreased by about 68 % over the last 10 years [6], further cost reductions are needed to make solar thermal power plants competitive with other regenerative (wind, PV) and fossil energy technologies. An important aspect of cost reduction is material cost and durability. The development of Al $_2$ O $_3$ forming stainless steels with high mechanical strength, especially fatigue resistance, offers the potential for cost-effective structural material solutions. In the development of a cost-effective alternative, it is also important to ensure that it has good resistance to the heat transfer fluid used.

The aim of the presented alloy development was to combine the strengthening by precipitation of intermetallic Laves phase particles, known from ferritic "HiperFer" [7], [8] alloys, with the formation of a salt corrosion resistant oxide surface layer. Laves phases form a large class of intermetallic compounds that have tended to be considered detrimental phases to

avoid [9]. However, with proper control of the precipitation process, the Laves phase can serve as strengthening particles [7], [8], [10], [11], [12]. The main Laves phase forming elements W, Nb, and Si strongly influence the mechanical properties by modification of the solid solution and precipitation strengthening effects. By using model alloys, 100 g each, alloying elements such as Al, Nb and W were varied to investigate the influence of alloy chemistry on Al_2O_3 formation and the precipitation of fine, long-term stable Laves phase particles in the ferrite matrix. Following the experiments detailed microstructure investigation of the chemistry (EDX) and of the surface layer formation (FE-SEM) was carried out. Furthermore, first results of fatigue experiments under superimposed salt corrosion attack at 600 °C will be presented.

Materials and Methods

Materials and Preparation

In this work, seven ferritic model alloys, 100 g each, were investigated. The Al content was varied to investigate the influence on the precipitation of the Laves phase, as well as the influence on the formation of the Al-oxide top layer, while the W and Nb contents were increased to examine the extent to which they influence the precipitation of the Laves phase. W, Nb and Si are used for combined solid solution and precipitation hardening. In FeCrAl alloys, Nb is an important component in the precipitation of the Laves phase [8], [13], [14] and at the same time prevents the formation of chromium carbides at grain boundaries, which can lead to intergranular corrosion [15]. The addition of W provides solid solution hardening and increases the volume fraction of the Laves phase [14]. The intermetallic (Fe,Cr,Si,Al)₂(Nb,W) Laves phase particles can significantly increase the mechanical strength of such alloys [16], [17]. The addition of Si promotes the formation of the Laves phase, stabilizes it [17], [18], and increases the service life of FeCrAl steel components by improving the adhesion of the protective oxide layers [19].

The model alloys were prepared under argon in a cold levitation crucible using high purity raw materials. The distribution of the alloying elements is largely homogeneous and no segregations were detected. The chemical compositions of the model alloys (analyzed by Inductively Coupled Plasma Optical Emission Spectroscopy (ICP-OES); C, S and N analyzed by infrared absorption) are given in Table 1.

Alloy Designation	С	S	N	Cr	Al	W	Nb	Si	Fe
2 Al	0.0032	< 0.0017	< 0.0003	17.25	1.904	2.58	0.61	0.21	R
3.5 Al	0.002	< 0.0022	< 0.0003	17.25	3.41	2.93	0.7	0.259	R
5 Al	0.0011	< 0.002	< 0.0003	17.3	4.917	2.74	0.638	0.224	R
8 Al	0.0054	< 0.002	< 0.0003	17.1	7.84	2.79	0.671	0.255	R
14 AI	< 0.001	< 0.0022	< 0.0003	17.0	13.9	2.78	0.673	0.258	R
4W 1Nb 3.5Al	0.0026	< 0.0018	< 0.0003	17.1	3.56	4.04	1.05	0.236	R
4W 1Nb 5Al	0.006	< 0.0022	< 0.0003	17.2	5.04	4.22	1.09	0.247	R

Table 1. Chemical composition (wt.%) of the ferritic model alloys.

After solution annealing, specimens with dimensions of 10 mm x 10 mm x 1 mm were taken from the melts by electrical discharge machining. In accordance with ISO 17245:2015 [20], the surfaces and edges of these specimens were ground with 600-grit SiC paper to ensure comparable initial conditions for surface roughness. Finally, the specimens were cleaned with ethanol and dried with hot air. In air, temperatures of at least 1000 °C or higher are normally required for the formation of a protective $\alpha\text{-Al}_2\text{O}_3$ layer on metal surfaces of FeCrAl alloys [20], [21]. At temperatures above 1350 °C, much faster oxidation kinetics can occur, determined by formation of iron oxides [20]. To also investigate the corrosion attack of the solar salt on a preformed Al₂O₃ layer, one sample per model alloy was annealed at 1100 °C / 1 h in laboratory air. The temperature was selected to prevent uncontrolled precipitation of particles of the Laves

phase, which can occur below 1050 °C [17]. SEM and a photograph of each model alloy before exposure to solar salt are shown in Figure 1. In the pre-oxidized model alloys 4W1Nb3.5Al and 4W1Nb5Al, coarse Laves phase precipitates are still present. Due to the increased W and Nb contents, pre-oxidation temperatures of more than 1100 °C are apparently necessary to prevent uncontrolled precipitation of the Laves phase. After heat treatment tests, suitable pre-oxidation parameters (1175 °C /1 h) could be determined for these two model alloys, too.

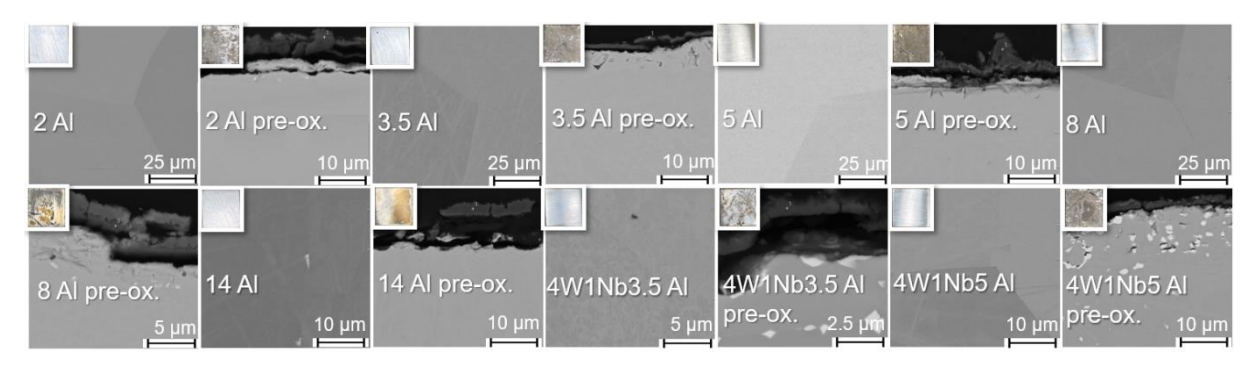


Figure 1. SEM of the specimen before corrosion testing.

The development and qualification of innovative experimental methods for fatigue testing under superimposed salt corrosion attack was carried out on the commercial materials TP347H and DMV 310N (Table 2). Cylindrical, salt-filled hollow specimens are used for this purpose. The geometry (in terms of wall thickness) and surface roughness (inside and outside of the specimen) were adjusted so that the fatigue damage starts from the inside of the specimen and occurs within the gauge length. This was successfully verified by fatigue tests on salt-filled and pre-corroded 347H specimens.

Table 2. Composition of alloys used for fatigue testing.

Alloy Designation	С	Si	Mn	Р	S	Cr	Ni	Nb	N	W	Мо	Fe
TP347H	0.10	1.00	2.0	0.045	0.030	19.0	13.0	-	-	-	4.00	R
DMV 310N	0.10	0.75	2.00	0.030	0.030	26.0	23.0	0.60	0.35	-	-	R

Experimental methods

Discontinuous salt corrosion testing of alloy specimens, placed inside salt-filled alumina crucibles, was carried out for a total of 2000 h at 600 °C in synthetic air (flow rate: 10 sl/h), flushed through the tube furnace. For this study, a mixture of 60 wt.% NaNO₃ (supplier: BASF SE, Ludwigshafen, Germany) and 40 wt.% KNO₃ (supplier: Haldor Topsoe, Lyngby, Denmark) was prepared. Because the solar salt creeps out of the specimen containers with aging time, fresh solar salt is replenished every 500 h to ensure continuous coverage of the alloy specimens. The specimens were weighed every 250 h to calculate their individual mass changes according to DIN 50905-1 [22]. For investigating the effect of superimposed salt attack on fatigue properties hollow, cylindric specimens were filled with solar salt and pre-aged for 500 h at 600 °C before the fatigue experiments. Further details regarding equipment and testing methodology for fatigue testing [8] and salt corrosion behavior [9] are described in the literature.

Results and Discussion

Discontinuous corrosion testing

For the model alloy with the lowest Al content of 2 wt.% (2 Al) a strong mass increase of about 0.875 mg/cm² was encountered in the first 250 h (cf. Figure 2a). After 500 h of ageing in solar salt, a strong net loss of about 1.375 mg/cm² became evident. These mass losses, which are even higher in case of the pre-oxidized 2 Al, result from spallation of the oxide layer and indicate insufficient adhesion to the base material. Obviously, the Al content of 2 wt.% is too low to form a protective top layer. The fact that Al is simultaneously consumed by the precipitation of Laves phase within the ferrite matrix may play a worsening role in this instance. After 750 h, only minor mass changes occur. Except for 4W1Nb3.5Al (cf. Figure 2c), this also applied to all other model alloys.

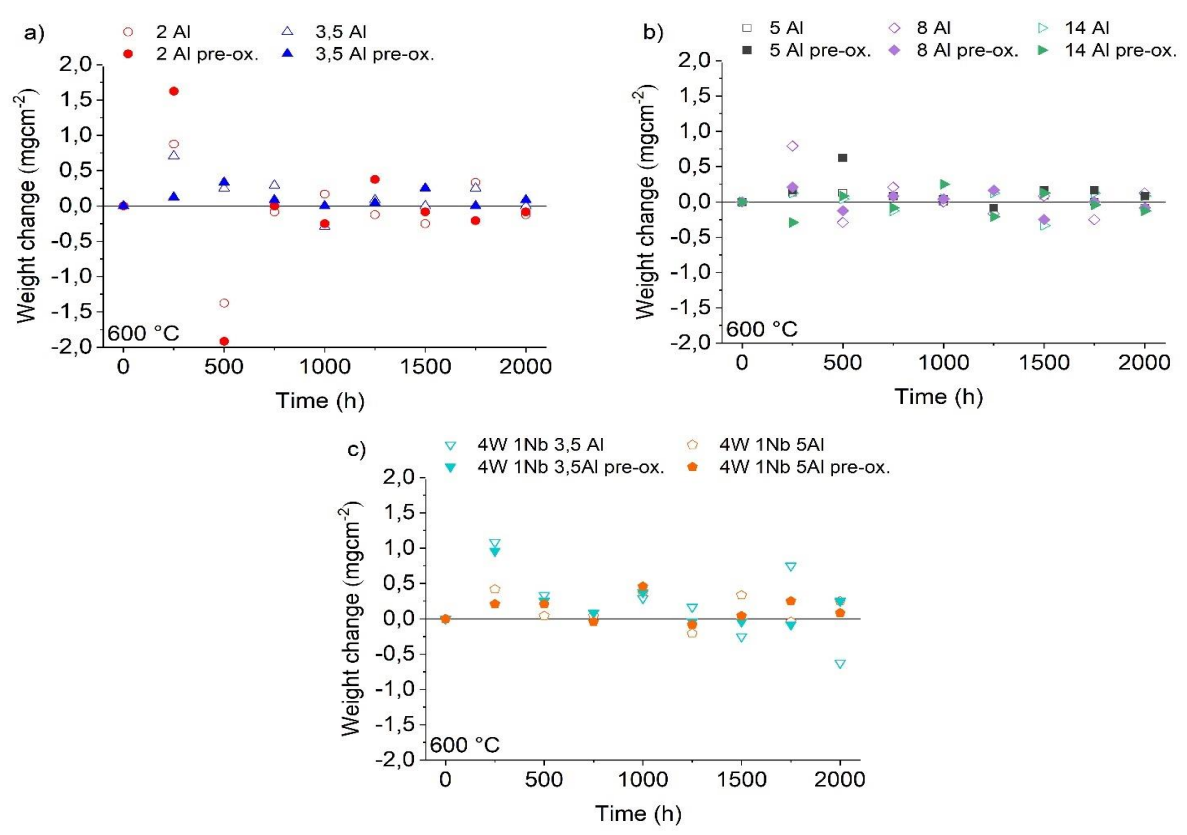


Figure 2. Weight changes of corrosion specimens during discontinuous annealing in solar salt at 600 °C: a) low Al content, b) high Al content and c) high W and Nb content.

In comparison to the 2 Al alloy, the mass gain/loss of 3.5 Al was relatively low. The slight increase in mass gain for the 3.5 Al alloy in the first 500 h indicates uniform, slow oxide film growth. This can also be observed for the model alloys with increased Al content (cf. Figure 2b). When considering the mass changes of the model alloys with varying Al content, preoxidation was demonstrated to be detrimental due to the increased mass change. The increase of W and Nb contents in combination with an increase in Al content from about 3.5 wt.% to about 5 wt.% seems to cause a lower mass change (cf. Figure 2c). After the first 250 h, the mass increase of 4W1Nb3.5Al with 1.083 mg/cm² was about three times higher than that of 4W1Nb5Al. At the end of the 2000 h of aging, 4W1Nb3.5Al still exemplified higher mass losses due to spallation of the oxide layer. Comparing the weight changes of 4W1Nb3.5Al and 4W1Nb5Al, it can be concluded that the increased W and Nb contents, because of the interaction of oxide layer growth and Laves phase precipitation, also necessitate increased Al content to obtain a slow-growing oxide layer. Just a limited influence of the Al content on the mass change can be recognized. An Al content of 3.5 wt.% and above ensures a consistently low mass change. With increased W and Nb contents, an Al content of 5 wt.% is necessary

for this effect. Higher W and Nb contents therefore require higher Al contents to ensure sufficient availability of Al for the formation of a stable Al₂O₃ top oxide layer. This shows further optimization potential regarding improved strength (due to higher W and Nb contents [23]), while maintaining high salt corrosion resistance.

Surface examination results (with associated light photographic images of the specimen surfaces) are presented in Figure 3. Looking at the photograph, the oxide layer appears reddish-brown for the specimens with AI contents up to 3.5 wt.% and increased W and Nb contents, which indicates an Fe-rich oxide layer. At an AI content from 5 wt.% to 14 wt.% the sample surfaces appear grayish-beige, which indicate an AI-containing oxide layer. For the model alloys with AI contents up to 3.5 wt.%, on which bulky multi-layer Na-Fe-oxides formed, the SEM show indications of spallation, but no superficial cracks. This is consistent with the findings from the weight change curves (cf. Figure 2). With higher AI content, the oxide layer turns to a fine-grained morphology with fewer bulges, consisting of mixed Na,-Fe oxide, forming on top of a mixed AI-Cr-Fe oxide layer. On the pre-oxidized specimen, the oxide layer appears coarser. On 14 AI only, mixed AI-oxide without bulges of Na-Fe-oxide were detected. In the sample cross-section of the 14 AI alloy (cf. Figure 4), a protective, continuous AI_2O_3 layer with a thickness of about 40 nm has formed after 2000 h at 600 °C in solar salt. In contrast to the other model alloys the 14 AI specimen did not form Laves phase in the base metal during aging in solar salt.

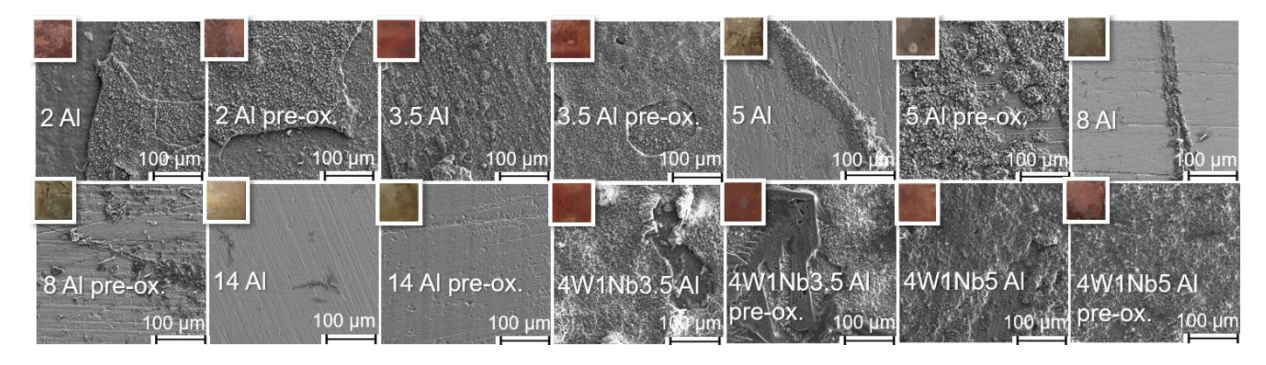


Figure 3. SEM of the specimen surfaces after 2000 h of discontinuous corrosion testing in solar salt at 600 °C (inlay light optical photographs showing specimen surface color)

The EDX-element mappings of the cross sections of specimen with an Al content of 2 wt. % and 8 wt. % are shown in Figure 5. For the alloys with Al contents of up to 3.5 wt. %, higher W and Nb content and pre-ox. 5 Al (cf. Figure 5), the oxide layer forms in three layers: An intermediate layer of Cr-Na-Fe-oxide formed between an upper layer of Na-Fe mixed oxide and a bottom layer of Cr-Al oxide on the steel substrate. This type of three-layer oxide film formation is already known from previous salt corrosion experiments with ferritic FeCrAl alloys [9]. Coarse AlN precipitates can only be found below all multilayer oxide areas.

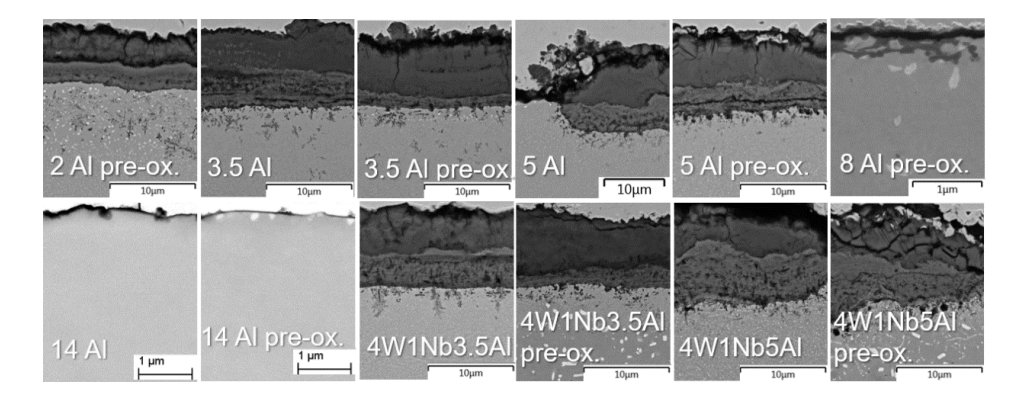


Figure 4. Scanning electron micrographs of the specimen cross sections after 2000 h of discontinuous corrosion testing in solar salt at 600 °C

For 5 Al the multilayer oxide formation was only observed in the few bulky areas. In the flat areas, a thin and compact Al_2O_3 layer was found in case of the 5 Al and 8 Al alloy. Because of pre-oxidation the oxide layer of pre-ox. 8 Al appears to be incomplete and thus permeable to the solar salt. This leads to internal oxidation by Na. It is remarkable that a protective Al_2O_3 layer forms in the solar salt at the moderate temperature of 600 °C, even without pre-oxidation in air, as was seen previously in corrosion experiments in solar salt at the same aging temperature with similar alloy composition [9]. This means that the alloy concept with all the tested variations of Al, W and Nb is potentially self-passivating upon exposure to solar salt.

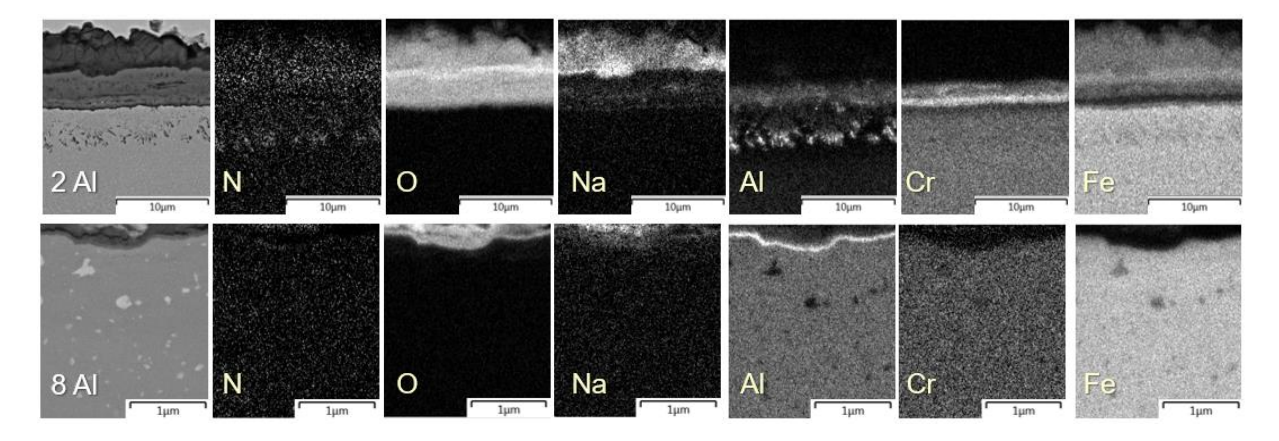


Figure 5. EDX-element mappings of the cross-sections of specimen with Al content of 2 wt. % and 8 wt. % after 2000 h of discontinuous corrosion testing in solar salt at 600 °C

Fatigue testing

Experimental technique

To evaluate the fatigue performance of structural materials under realistic molten salt corrosion conditions is a challenging task, which has to address two main experimental difficulties:

- The molten salt has to be safely sealed within the testing set-up to avoid health issues for operating personnel and
- the chemical stability of the salt melt has to be maintained over the experimental duration. Molten salt solar receivers typically feature receiver tubes with wall thicknesses in the low (e.g. 1 to 4) millimeter range.

For this reason, several possible interrelations have to be addressed when designing a realistic testing method: Wall thickness of the tube may have a direct impact on corrosion lifetime, because it

- determines the reservoir of corrosion inhibiting species within the alloy matrix.
- In case of austenitic and Ni-base alloys, grain size (especially in relation to wall thickness) may be another decisive factor. The comparatively low diffusion velocities in the fcc matrix type make grain boundary diffusion an important factor in the corrosion performance of these alloys.

Hollow, salt-filled fatigue testing specimens (Figure 6), which replicate the wall thickness of the actual receiver tube, are a practical way to solve these main issues and to achieve realistic results.

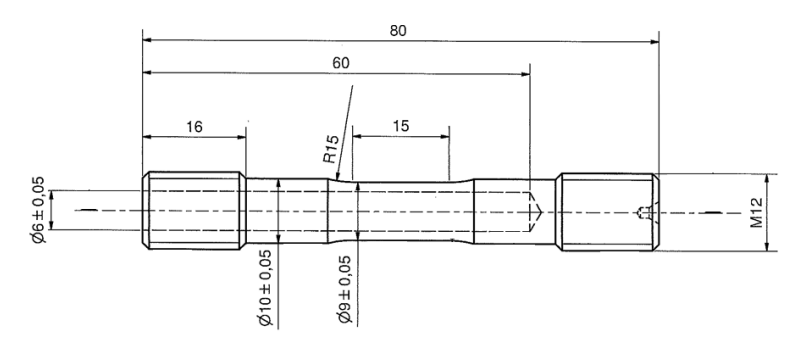


Figure 6. Hollow, cylindrical fatigue testing specimen geometry applied at FZ Jülich, IEK-2.

To yield reliable fatigue performance data the testing technique has to mimic realistic corrosion attack and fatigue failure. i.e.

- initiation of fatigue cracking within the gauge length and at the inner specimen wall (which is in contact with the molten salt) has to be ensured by specimen geometry and surface preparation. This is achieved by machining the inner wall to a surface roughness, typical for a commercial tube (R_a / R_z: 0,20 0,45 μ m / 1,9 3,5 μ m) and sub-micron, mirror polishing of the outer wall gauge section (R_a / R_z: 0,04 0,09 μ m / 0,2 0,8 μ m).
- As corrosion takes time, the choice of experimental parameters must provide sufficient testing duration for corrosive attack at the inner wall surface.
- Suitable specimen pre-corrosion treatment procedures may be necessary, especially if local (pitting) corrosion plays a role, because under high mechanical loading (i.e. high strain range testing) experimental duration may not be sufficiently long for corrosion to occur. Nevertheless, such parameter ranges are relevant for application and must be thoroughly tested for this reason.

Preliminary results and interpretation

Preliminary LCF testing (T: 600° , $d\epsilon/dt$: $10^{-3}s^{-1}$, $\Delta\epsilon$: +/- 0,25 %) results from T/P347H indicate a negative impact of salt corrosion attack (Fig. 7a). While hollow specimens without salt filling reached lifetimes of about 26.500 +/- 1.000 cycles, superimposed salt corrosion (hollow, salt filled specimen) yielded a reduction to less than half the lifetime. Interestingly, isothermal salt pre-corrosion treatment (T: 600° , t: 670 h) resulted in earlier crack initiation, prevented cyclic hardening and consequently caused further reduction in lifetime to less than 10.000 cycles.

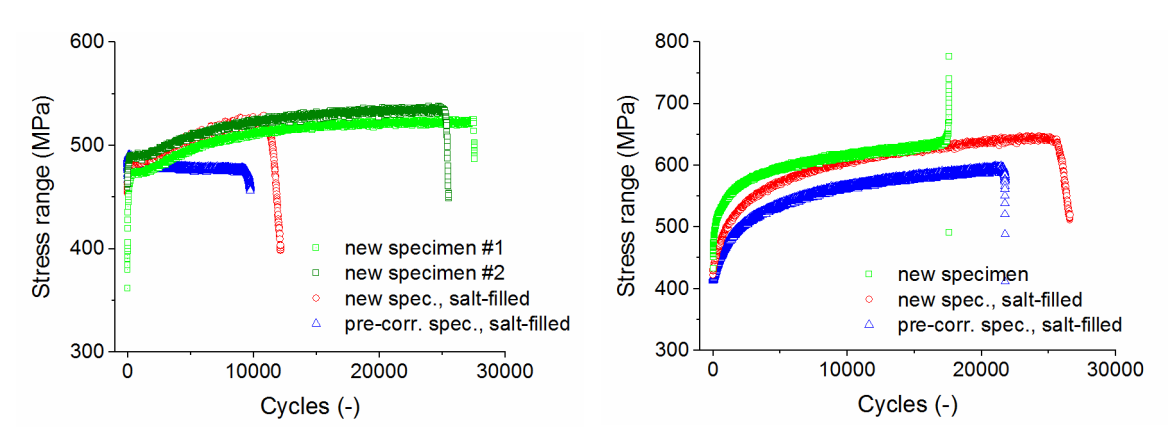


Figure 7. Impact of salt(-pre) corrosion on the fatigue curves of commercial austenitic (a) T/P347H and (b) 310N steel (T: 600° , $d\epsilon/dt$: $10^{-3}s^{-1}$, $\Delta\epsilon$: +/- 0,25 %).

In contrary, superimposed salt corrosion (new, salt-filled specimen, Fig. 7b) resulted in increased fatigue life in case of alloy 310N. Isothermal salt pre-corrosion (pre-corroded, salt-filled specimen, Fig. 7b) caused a reduction in comparison to the salt-corrosion only condition, but still yielded longer life. The reason for this difference in behavior is suspected to be related

to the higher Ni-and Cr-contents (cf. Tab. 2) of the 310N alloy, which potentially make it more stable towards molten salt attack. The active damage mechanisms, especially molten salt / crack-tip interactions, still have to be examined by detailed microstructural post-mortem analysis of the tested specimens.

Conclusion

The key results of the salt corrosion experiments can be summarized as follows:

- For low Al content of up to 3.5 wt.% spallation of the formed surface oxide occurs. The
 oxide forms in three layers: An intermediate layer of Cr-Na-Fe-oxide between an upper
 layer of Na-Fe mixed oxide and a bottom layer of Cr-Al oxide adjacent to steel
 substrate.
- Coarse AlN precipitates can be found below the oxide layer for an Al content up to 5 wt.%. As expected, intermetallic phase precipitates of Fe, Cr, Al, W and Nb form in the base metal.
- 14 Al forms a protective, continuous Al₂O₃ layer with a thickness of about 40 nm but does not form Laves phase in the base metal during aging in solar salt.
- Pre-oxidation is detrimental due to increased mass changes and coarse, discontinuous oxide layer.
- Increased W and Nb contents necessitate higher Al content to obtain slow-growing oxide layer due to the interaction of oxide layer growth and Laves phase precipitation.
- Protective Al₂O₃ layers form in solar salt at the moderate temperature of 600 °C, even without pre-oxidation in air. The alloying concept (in all the tested variations of Al, W and Nb contents) is potentially self-passivating upon exposure to solar salt.

The key results of the fatigue experiments under superimposed salt corrosion are:

- The presented specimen geometry and treatments of the inner and outer surfaces ensure crack initiation at the inner surface, which is exposed to molten salt.
- Fatigue behavior of structural materials under superimposed attack by molten salts differs with alloy composition.
- Fatigue results cannot be interpreted without detailed microstructural post-mortem analysis of the fatigued specimens.

Data availability statement

Data sharing is not applicable.

Underlying and related material

No underlying or related material available.

Author contributions

Conceptualization, F.A. and B.K.; methodology, F.A. and B.K., investigation, F.A.; resources, B.K.; data curation, F.A.; writing—original draft preparation, F.A.; writing—review and editing, B.K., and F.A.; visualization, F.A. and B.K.; supervision, B.K.; project administration, B.K.; funding acquisition, B.K. All authors have read and agreed to the published version of the manuscript.

Competing interests

The authors declare no competing interests.

Funding

This work was funded by the German Federal Ministry of Education and Research (BMBF) under grant number 03EE5048A, which is greatly appreciated.

Acknowledgement

The authors also wish to thank the following staff members of Forschungszentrum Jülich GmbH: E. Wessel and D. Grüner (microstructural examination).

References

- R. Guédez, M. Topel, J. Spelling, B. Laumert, "Enhancing the Profitability of Solar Tower Power Plants through Thermoeconomic Analysis Based on Multi-objective Optimization," Energy Procedia, 69, pp. 1277 – 1286, 2015, DOI: 10.1016/j.egypro.2015.03.155
- 2. F. Zaversky, J. García-Barberena, M. Sánchez, D. Astrain, "Transient molten salt two-tank thermal storage modeling for CSP performance simulations," Solar Energy, 93, pp. 294-311, 2013, DOI: 10.1016/j.solener.2013.02.034
- 3. A. Bonk, C. Martin, M. Braun, T. Bauer, "Material investigations on the thermal stability of solar salt and potential filler materials for molten salt storage," AIP Conference Proceedings, 1850, 080008, pp. 1-8, 2019, DOI: 10.1063/1.4984429
- 4. A.M. Kuizenga, J.G. Cordaro, "Preliminary Development of Thermal Stability Criterion for Alkali Nitrates," Sandia Technical Report SAND2011-5837C; Sandia National Laboratories: Albuquerque, NM, USA, 2011.
- 5. F. Aarab, B. Kuhn, A. Bonk, T. Bauer, "A New Approach to Low-cost, Solar Salt Resistant Structural Materials for Concentrating Solar Power (CSP) and Thermal Energy Storage (TES)," Metals 2021, 11, 1970, 2021, DOI: 10.3390/met11121970
- 6. IRENA, "Latest Cost Trends," in Renewable Power Generation Costs in 2020,", International Renewable Energy Agency, Abu Dhabi, 2021.
- 7. B. Kuhn, T. Fischer, X. Fan, M. Talik, M., F. Aarab, Y. Yamamoto, "HiperFer Weiterentwicklungs- und Anwendungspotenzial," FVWHT, 43, 2020.
- 8. B. Kuhn, M. Talik, T. Fischer, X. Fan, Y. Yamamoto, J. Lopez Barrilao, "Science and Technology of High Performance Ferritic (HiperFer) Stainless Steels," Metals 2020, 10(4), 463, 2020, DOI: 10.3390/met10040463
- F. Stein, A. Leineweber, "Laves phases: a review of their functional and structural applications and an improved fundamental understanding of stability and properties," Journal of Materials Science, 56, pp. 5321–5427, 2021, DOI: 10.1007/s10853-020-05509-2
- J. Hald, "Microstructure and long-term creep properties of 9–12% Cr steels," International Journal of Pressure Vessels and Piping, 85, pp. 30-37, 2008, DOI: 10.1016/j.ijpvp.2007.06.010
- 11. S. Kobayashi, K. Kimura, K. Tsuzaki, "Interphase precipitation of Fe2Hf Laves phase in a Fe–9Cr/Fe–9Cr–Hf diffusion couple," Intermetallics, 46, pp. 80-84, 2014, DOI: 10.1016/j.intermet.2013.10.017
- 12. S. Kobayashi, "Formation of the Fe2Hf Laves Phase through Eutectoid Type Reaction of δ→γ+Fe2Hf in Ferritic Heat Resistant Steels," ISIJ International, Vol. 55 (2015), No. 1, pp. 2, 2014, DOI: 10.2355/isijinternational.55.293
- 13. B. Kuhn, M. Talik, L. Niewolak, J. Zureka, H. Hattendorf, P.J.Ennis, W.J. Quadakkers, T. Beck, L. Singheiser, "Development of high chromium ferritic steels strengthened by

- intermetallic phases," Materials Science and Engineering A, 594, pp. 372–380, 2014, DOI: 10.1016/j.msea.2013.11.048
- X. Fan, B. Kuhn, J. Pöpperlová, W. Bleck, U. Krupp, "Compositional Optimization of High-Performance Ferritic (HiperFer) Steels—Effect of Niobium and Tungsten Content, "Metals 2020, 10, 1300, 2020, DOI: 10.3390/met10101300
- 15. M. Żuk, A. Czupryński, D. Czarnecki, T. Poloczek, "The effect of niobium and titanium in base metal and filler metal on intergranular corrosion of stainless steels," Weld. Tech. Rev., 91, 6, pp. 30-38, 2019, DOI: 10.26628/wtr.v91i6.1032
- 16. T. Beck, B. Kuhn, T. Eckardt, L. Singheiser, "Microstructure, Creep and Thermomechanical Fatigue of Novel Solid Solution and Laves Phase Strengthened Cr2O3 and Al2O3 Forming Ferrites for Car Engine Exhaust and Heat Exchanger Systems," Trans Indian Inst Met, 69, pp. 379–385, 2016, DOI: 10.1007/s12666-015-0747-x
- 17. J.K. Lopez Barrilao, B. Kuhn, E. Wessel, "Microstructure and intermetallic particle evolution in fully ferritic steels," Proceedings of the 8th International Conference on Advances in Materials Technology for Fossil Power Plants, Albufeira, Portugal; Oct 11th 14th: pp. 1029–1037, 2016.
- 18. J. K. Lopez Barrilao, "Microstructure Evolution of Laves Phase Strengthened Ferritic Steels for High Temperature Applications," Energie & Umwelt, 375, 2017.
- 19. J. Klöwer, "Factors affecting the oxidation behaviour of thin Fe-Cr-Al foils Part II: The effect of alloying elements: Overdoping," Materials and Corrosion, 51, 5, pp. 373–385, 2000, DOI: 10.1002/(SICI)1521-4176(200005)51:5<373::AID-MACO373>3.0.CO;2-O
- 20. C. Kim, C. Tang, M. Grosse, M. Steinbrueck, C. Jang, Y. Maeng, "Oxidation Kinetics of Nuclear Grade FeCrAl Alloys in Steam in the Temperature Range 600-1500 °C," Proceedings of TOPFUEL 2021 Conference, Santander, Spain, Oct 24th – 28th, 2021, DOI: 10.5445/IR/1000145733
- 21. K. O. Gunduz, A. Visibile, M. Sattari, I. Fedorova, S. Saleem, K. Stiller, M. Halvarsson, J. Froitzheim, "The effect of additive manufacturing on the initial High temperature oxidation properties of RE-containing FeCrAl alloys," Corrosion Science, 188, 109553, 2021, DOI: 10.1016/j.corsci.2021.109553
- 22. Deutsches Institut für Normung e.V. Deutsches Institut für Normung e.V., DIN 50905-1, Korrosion der Metalle Korrosionsuntersuchungen: Teil 1: Grundsätze: Beuth Verlag GmbH; 2009, (DIN 50905-1).
- 23. G. Chen, H. Wang, H. Sun, Y. Zhang, P. Cao, J. Wang, "Effects of Nb-doping on the mechanical properties and high-temperature steam oxidation of annealing FeCrAl fuel cladding alloys," Materials Science and Engineering: A, 803, 140500, 2021, DOI: 10.1016/j.msea.2020.140500